

An observation-based constraint on permafrost loss as a function of global warming.

S. E. Chadburn^{*1,2}, E. J. Burke², P. M. Cox³, P. Friedlingstein³, G. Hugelius⁴ & S. Westermann⁵

¹*University of Leeds, School of Earth and Environment, LS2 9JT, UK*

²*Met Office Hadley Centre, FitzRoy Road, Exeter, EX1 3PB, UK*

³*University of Exeter, Earth System Science group, North Park Road, EX4 4QE, UK*

⁴*Stockholm University, Institutionen för naturgeografi, 106 91 Stockholm, Sweden*

⁵*University of Oslo, Department of Geosciences, P.O. Box 1047 Blindern, NO-0316 Oslo, Norway*

Permafrost, which covers 15 million km² of the land surface, is one of the components of the Earth System that is most sensitive to warming^{1,2}. Loss of permafrost would radically change high-latitude hydrology and biogeochemical cycling, and could therefore provide very significant feedbacks on climate change³⁻⁸. The latest climate models all predict warming of high-latitude soils and thus thawing of permafrost under future climate change, but with widely varying magnitudes of permafrost thaw^{9,10}. Here we show that in each of the models, their present-day spatial distribution of permafrost and air temperature can be used to infer the sensitivity of permafrost to future global warming. Using the same approach for the observed permafrost distribution and air temperature, we estimate a sensitivity of permafrost area loss to global mean warming at stabilisation of $4.0_{-1.1}^{+1.0}$ million km² °C⁻¹ (1σ confidence), which is around 20% higher than previous studies⁹. Our method facilitates an assessment for COP21 climate change targets¹¹: If the climate is stabilised at 2°C above pre-industrial

21 **levels, we estimate that the permafrost area would eventually be reduced by over 40%. Sta-**
22 **bilising at 1.5°C rather than 2°C would save approximately 2 million km² of permafrost.**

23 Permafrost, defined as ground that remains at or below 0°C for two or more consecutive
24 years, occurs on 24% of the land in the Northern hemisphere ¹². Under recent climate warming,
25 permafrost has begun to thaw, causing changes in ecosystems and impacting northern communities,
26 for example through collapse of roads and buildings as the ground becomes unstable ¹³. Large
27 quantities of carbon are stored in organic matter in permafrost soils ¹⁴, which starts to decompose
28 when the permafrost thaws, resulting in the emission of greenhouse gases such as carbon dioxide
29 and methane. In future, carbon release from permafrost thaw may have a significant impact on
30 the Earth's climate ⁶. Due to its global importance, numerous modelling studies have assessed
31 the rate of permafrost thaw under future climate warming ^{9,10,15,16}. However, despite progress in
32 process-based modelling on local and regional scales e.g. ¹⁷, a lack of data availability and model
33 deficiencies mean that permafrost is still poorly simulated in global climate models, where the
34 historical simulations show a present-day permafrost area anywhere between 0.1 and 1.8 times the
35 size of that observed ⁹. Models often have shallow soil columns, a limited representation of soil
36 properties, inadequate snow thermal and physical dynamics and other missing processes ⁹. Here
37 we present a projection of large-scale permafrost thaw that is based on observations, avoiding
38 model bias, and accounting for observational uncertainty.

39 Our approach is based on using the relationship between mean annual air temperature (MAAT)
40 and permafrost occurrence to estimate permafrost extent. Permafrost is not exclusively determined

41 by air temperature, being strongly influenced by landscape features such as topography, soil ther-
42 mal properties, snow depth and hydrology ¹⁸. Nonetheless it is possible to construct a broad re-
43 lationship between MAAT and the presence of permafrost, defined in terms of the probability
44 of finding permafrost at a given air temperature ¹⁹. Averaged over large spatial scales, proba-
45 bility translates to the areal fraction underlain by permafrost. We derived a MAAT-permafrost
46 relationship using a robust approach that integrates the spatial distribution of permafrost from the
47 International Permafrost Association (IPA) map of permafrost in the Northern hemisphere ²⁰.

48 The observation-based IPA map defines the spatial boundaries of the permafrost zones: Con-
49 tinuous, >90% coverage; discontinuous, 50-90% coverage; sporadic, 10-50% coverage; isolated
50 patches, 0-10% coverage. We took the air temperatures at the spatial permafrost boundaries and
51 fitted them against the respective permafrost fractions. The resulting relationship between MAAT
52 and permafrost fraction is shown in Figure 1a. We also provide a plausible range, which covers
53 different sources of uncertainty. Firstly, the range of air temperatures for a given permafrost frac-
54 tion indicates variability due to large-scale differences in snow depth, soil moisture, landscape type
55 etc.; Secondly, uncertainties in the IPA map are incorporated by including air temperatures from
56 100km either side of each boundary. Detailed evaluation of this relationship by validation against
57 local field data and regional modelling suggests that it is robust (Figure S1). More details are given
58 in the Supplementary discussion.

59 We used this relationship between MAAT and permafrost to reconstruct the IPA permafrost
60 map from WATCH reanalysis air temperatures (using the 1960-1990 period, consistent with the

61 IPA observational window) ^{21,22}, Figure 1b,c. The estimated permafrost area is 15.5 million km²
62 using this technique (12.0-18.2 million km² using minimum/maximum curves), which compares
63 well with 15.0 million km² from observations ²⁰ (12.6-18.4 million km²). A spatial correlation
64 between observed and estimated permafrost extent has an r² value of 0.85. Note that this area
65 refers to the actual area of permafrost, whereas the larger value given in ¹² includes the total area
66 of all permafrost zones (e.g. including the whole sporadic zone, of which only a small fraction is
67 actually permafrost).

68 Figure 1d,e shows the maximum and minimum permafrost distributions according to the lim-
69 iting curves on Figure 1a. It is clear that any major discrepancy between the observed distribution
70 and our estimate is covered by the maximum and minimum distributions (see also Fig. S8). One
71 of the major causes of such discrepancies is snow, which insulates the ground in winter ²³. We
72 included the influence of factors such as snow and ground thermal properties in the limiting curves
73 instead of spatially resolving them ^{15,24}, in order to account for the full range of uncertainties in
74 future projections.

75 We applied this relationship (Fig. 1a) to make projections of future permafrost extent. Our
76 approach calculates the committed permafrost distribution for each global mean temperature. Dur-
77 ing a period of warming, the actual changes in permafrost area will lag behind this quasi-equilibrium
78 state, due to the long time-scale of warming for the deep ground. However, our analysis has high
79 relevance to international climate negotiations, which are framed in terms of climate stabilisa-
80 tion. We can, for example, estimate the relative impacts of stabilising at 1.5°C or 2°C above

81 pre-industrial levels ¹¹.

82 Coupled models provide the best available indication of whether the relationship between
83 MAAT and permafrost will fundamentally shift in the future (for example, if there is a pan-Arctic-
84 scale change in snow depth relative to air temperature). We therefore test this using the CMIP5
85 climate model ensemble ²⁵, which provides a large dataset of coupled simulations. For each model
86 we derive a model-specific MAAT-permafrost relationship from the historical simulation (Fig. S3).
87 The robustness of our approach depends on the extent to which this relationship between per-
88 mafrost area and air temperature remains consistent under climate change. The transferability of
89 the Permafrost-Air Temperature (PF-Tair) relationship was assessed by comparing the relationship
90 derived from the models for the historical period 1960-1990, to that for the period 2270 to 2300
91 (Figure S4). The PF-Tair curves for these two periods are generally very similar, and always within
92 our uncertainty bounds. This is one of the main reasons that our approach is robust, as it is valid in
93 every case despite the fact that the models differ in their representation of the key processes and in
94 the details of their projections. We then estimated the future permafrost area, using the historical
95 MAAT-permafrost relationships and future air temperatures from each model (Figure 2a), includ-
96 ing 9 coupled climate models used in the latest IPCC assessment ²⁶, and two different emission
97 scenarios. The area is accurately estimated in every case.

98 We applied the same technique using the ‘true’ observationally-derived MAAT-permafrost
99 curve (Fig. 1a) to make projections of future permafrost area that are constrained by observations.
100 In order to be independent of specific climate models and emission scenarios, we reduced the future

101 air temperature changes down to just two variables: global mean warming, and Arctic amplification
102 as a function of latitude. For this we used a pattern-scaling technique, in which air temperatures are
103 increased by the global mean warming multiplied by the Arctic amplification. Arctic amplification
104 is the phenomenon caused by changing surface albedo due to the melting of snow and ice, in which
105 air temperatures in the Arctic warm approximately twice as fast as the global mean²⁶. We estimate
106 the amplification factor as a function of latitude, from the observed historical warming trend (1936-
107 2012), using the WATCH reanalysis air temperature data^{21,22}. The observed amplification factor
108 differs substantially from models²⁷ (Figure S5) which is a good reason for using this approach
109 rather than simulated future air temperatures (see Methods for further discussion).

110 The CMIP5 models were used to test the consistency of this technique. Using the same in-
111 formation from the models that is available for the real world (Arctic amplification derived from
112 historical simulations (1936-2012), and global mean warming), we estimate the future air tempera-
113 tures for each model. From these we again use the model-specific MAAT-permafrost relationships
114 to estimate future permafrost area. This gives projections of future permafrost area that agree with
115 the simulated permafrost areas within the uncertainty for all models, Fig. 2b.

116 We can therefore apply our methodology using observational data alone, namely observed
117 present-day air temperature, historical Arctic amplification, and the observed MAAT-permafrost
118 relationship (Figure 1a), to estimate global permafrost loss for a given level of future global warm-
119 ing.

120 Using our approach, the loss of permafrost under stabilisation, as a function of the global

121 mean warming, is $4.0_{-1.1}^{+1.0}$ million $\text{km}^2 \text{ } ^\circ\text{C}^{-1}$ (note that all uncertainties are quoted at 1σ level.)
122 Under a $1.5 \text{ } ^\circ\text{C}$ stabilisation scenario, $4.8_{-2.2}^{+2.0}$ million km^2 of permafrost would be lost compared
123 with the 1960-1990 baseline (corresponding to the IPA map, Figure 1b), and under a $2 \text{ } ^\circ\text{C}$ stabili-
124 sation we would lose $6.6_{-2.2}^{+2.0}$ million km^2 , over 40% of the present-day permafrost area. Therefore,
125 stabilising at $1.5 \text{ } ^\circ\text{C}$ rather than $2 \text{ } ^\circ\text{C}$ could potentially prevent approximately 2 million km^2 of
126 permafrost from thawing. The loss of permafrost with warming is shown on Figure 3 for a wide
127 range of scenarios. Our results indicate that for the high warming scenarios (5 or 6°C above pre-
128 industrial - similar to the warming in RCP8.5 by 2100 ²⁶), the vast majority of permafrost will
129 thaw, leaving only 0.3 - 3.1 million km^2 under 5°C of warming and 0.0 - 1.5 million km^2 under 6°C .
130 Even accounting for the uncertainties due to heterogeneity in air temperature, snow, etc., we have
131 greatly reduced the range from the unconstrained model ensemble (shown on Figure 3).

132 Our approach also enables a broad spatial assessment of permafrost vulnerability, which is
133 difficult with Earth System Models due to problems with their simulation of the current permafrost
134 distribution ⁹. Figure 4 shows the estimated spatial pattern of high-latitude permafrost historically
135 (1960-1990), and the range of the zonal boundaries under 1.5°C stabilisation (Figure 4a) and 2°C
136 stabilisation (Figure 4b). Thawing permafrost has direct impacts on people and infrastructure in
137 the areas where it thaws. 35 million people live in the permafrost zone ^{28,29}, including in three
138 cities (population $>100,000$) built on continuous permafrost (marked on Fig. 4). These cities, for
139 example, would most likely transition to the discontinuous permafrost zone under 2°C of warming,
140 putting their infrastructure at risk. Hydrological impacts vary with the depth of thaw but would
141 include localised ground collapse, lake formation and soil drainage. Note that due to the nature of

142 our approach, only large-scale spatial patterns of permafrost thaw are considered.

143 Previous estimates of permafrost sensitivity were generally given in terms of high-latitude
144 warming, rather than global warming. Previous published values are equivalent to 3.3 ± 1.2 mil-
145 lion $\text{km}^2 \text{ }^\circ\text{C}^{-1}$, based on the CMIP5 model simulations ⁹, and 1.8-2.6 million $\text{km}^2 \text{ }^\circ\text{C}^{-1}$ based
146 on an ensemble of offline model runs ¹⁶. These are smaller than our value of $4.0_{-1.1}^{+1.0}$ million km^2
147 $^\circ\text{C}^{-1}$ (although they fall within 1-2 σ of our estimate). The published values ^{9,16} are derived from
148 transient simulations, so the difference may be partly due to the transient effect, where permafrost
149 thaw ‘lags’ behind the climate warming, especially under scenarios such as RCP8.5 where the air
150 temperature changes very quickly. Indeed, a study using equilibrium permafrost models driven by
151 CMIP5 model output ¹⁰ showed that the equilibrium response is typically 25-38% greater than the
152 transient response, and in some models the difference was even larger (up to 70%). The major ad-
153 vantage of the approach adopted here is that committed permafrost loss, along with its uncertainty,
154 can be estimated for any policy-relevant global warming scenario.

155 We estimate the committed permafrost loss over the whole 20th century to be $3.4_{-2.3}^{+2.2}$ million
156 km^2 (until 2003-2012 ²⁶). Some of this committed change will not yet be observable, because
157 of the lag between the equilibrium and transient response. However, our estimate of permafrost
158 sensitivity to warming is consistent with observations of changes in near-surface permafrost, which
159 are expected to be much closer to equilibrium (see Supplementary Figures S6, S7 and discussion).
160 There may be longer-term transient effects, but these are relatively small (see Fig. S2).

161 This is the first study to quantify permafrost loss under policy-relevant climate stabilisation

162 scenarios, defined by the global warming. In particular we take an approach that is based on
163 observations and independent of climate model projections, reducing the problem of future sensi-
164 tivity down to only two key quantities: Arctic amplification and global mean temperature change.
165 Furthermore our constraint includes a comprehensive uncertainty bound, specifically giving a sen-
166 sitivity to global warming of $4.0_{-1.1}^{+1.0}$ million $\text{km}^2 \text{ } ^\circ\text{C}^{-1}$ at the 1σ level. This provides an important
167 benchmark for process-based global modelling. Using our approach we have analysed the differ-
168 ence between 1.5 and 2°C stabilisation, and shown that the committed permafrost loss is nearly
169 30% smaller at the lower stabilisation target, with relevance to climate negotiations surrounding
170 the Paris Agreement ¹¹.

- 172 1. Romanovsky, V. *et al.* Permafrost [in arctic report card 2013] (2013). URL
173 <http://www.arctic.noaa.gov/reportcard>.
- 174 2. Romanovsky, V., Burgess, M., Smith, S., Yoshikawa, K. & Brown, J. Permafrost temperature
175 records: Indicators of climate change. *Eos, Transactions American Geophysical Union* **83**,
176 589–594 (2002). URL <http://dx.doi.org/10.1029/2002E0000402>.
- 177 3. Grosse, G., Goetz, S., McGuire, A. D., Romanovsky, V. E. & Schuur, E.
178 A. G. Changing permafrost in a warming world and feedbacks to the
179 earth system. *Environmental Research Letters* **11**, 040201 (2016). URL
180 <http://stacks.iop.org/1748-9326/11/i=4/a=040201>.
- 181 4. Schaefer, K., Lantuit, H., Romanovsky, V. E., Schuur, E. A. G. & Witt, R. The impact of
182 the permafrost carbon feedback on global climate. *Environmental Research Letters* **9**, 085003

- 183 (2014). URL <http://stacks.iop.org/1748-9326/9/i=8/a=085003>.
- 184 5. Schneider von Deimling, T. *et al.* Estimating the near-surface permafrost-
185 carbon feedback on global warming. *Biogeosciences* **9**, 649–665 (2012). URL
186 <http://www.biogeosciences.net/9/649/2012/>.
- 187 6. Schuur, E. A. G. *et al.* Climate change and the permafrost carbon feedback. *Nature* **520**,
188 171–179 (2015). URL <http://dx.doi.org/10.1038/nature14338>.
- 189 7. MacDougall, A. H., Avis, C. A. & Weaver, A. J. Significant contribution to climate warm-
190 ing from the permafrost carbon feedback. *Nature Geoscience* **5**, 719–721 (2012). URL
191 <http://dx.doi.org/10.1038/ngeo1573>.
- 192 8. Burke, E. J., Hartley, I. P. & Jones, C. D. Uncertainties in the global temperature change
193 caused by carbon release from permafrost thawing. *The Cryosphere* **6**, 1063–1076 (2012).
194 URL <http://www.the-cryosphere.net/6/1063/2012/>.
- 195 9. Koven, C. D., Riley, W. J. & Stern, A. Analysis of permafrost thermal dynamics and response
196 to climate change in the cmip5 earth system models. *Journal of Climate* **26**, 1877–1900 (2013).
197 URL <http://dx.doi.org/10.1175/JCLI-D-12-00228.1>.
- 198 10. Slater, A. G. & Lawrence, D. M. Diagnosing present and future permafrost
199 from climate models. *Journal of Climate* **26**, 5608–5623 (2013). URL
200 <http://dx.doi.org/10.1175/JCLI-D-12-00341.1>.

- 201 11. United Nations Framework Convention on Climate Change, U. N. F. C. C. C. Adoption of
202 the paris agreement. *21st Conference of the Parties, Paris: United Nations* (2015). URL
203 <https://unfccc.int/resource/docs/2015/cop21/eng/l09r01.pdf>.
- 204 12. Zhang, T., Barry, R. G., Knowles, K., Heginbottom, J. A. & Brown, J. Statistics and character-
205 istics of permafrost and groundice distribution in the northern hemisphere. *Polar Geography*
206 **23**, 132–154 (1999). URL <http://dx.doi.org/10.1080/10889379909377670>.
207 <http://dx.doi.org/10.1080/10889379909377670>.
- 208 13. Schaefer, K., Lantuit, H., Romanovsky, V. & Schuur, E. A. G. *Policy Implications of Warming*
209 *Permafrost* (United Nations Environment Programme Special Report, Nairobi, Kenya, 2012).
210 URL <http://www.unep.org/pdf/permafrost.pdf>.
- 211 14. Hugelius, G. *et al.* Estimated stocks of circumpolar permafrost carbon with quantified un-
212 certainty ranges and identified data gaps. *Biogeosciences* **11**, 6573–6593 (2014). URL
213 <http://www.biogeosciences.net/11/6573/2014/>.
- 214 15. Anisimov, O. A. & Nelson, F. E. Permafrost zonation and climate change in the northern
215 hemisphere: Results from transient general circulation models. *Climatic Change* **35**, 241–258
216 (1997). URL <http://dx.doi.org/10.1023/A:1005315409698>.
- 217 16. Chadburn, S. E. *et al.* Impact of model developments on present and future simulations of
218 permafrost in a global land-surface model. *The Cryosphere* **9**, 1505–1521 (2015). URL
219 <http://www.the-cryosphere.net/9/1505/2015/>.

- 220 17. Westermann, S., Østby, T. I., Gislås, K., Schuler, T. V. & Etzelmüller, B.
221 A ground temperature map of the north atlantic permafrost region based on re-
222 mote sensing and reanalysis data. *The Cryosphere* **9**, 1303–1319 (2015). URL
223 <http://www.the-cryosphere.net/9/1303/2015/>.
- 224 18. Jorgenson, M. *et al.* Resilience and vulnerability of permafrost to climate
225 change. *Canadian Journal of Forest Research* **40**, 1219–1236 (2010). URL
226 <http://dx.doi.org/10.1139/X10-060>.
- 227 19. Gruber, S. Derivation and analysis of a high-resolution estimate of
228 global permafrost zonation. *The Cryosphere* **6**, 221–233 (2012). URL
229 <http://www.the-cryosphere.net/6/221/2012/>.
- 230 20. Brown, J., Ferrians Jr, O. J., Heginbottom, J. & Melnikov, E. Circum-arctic map of per-
231 mafrost and ground ice conditions. *National Snow and Ice Data Center* (1998). URL
232 http://nsidc.org/data/docs/fgdc/ggd318_map_circumarctic.
- 233 21. Weedon, G. P. *et al.* The watch forcing data 1958-2001: A meteorological forcing dataset
234 for land surface- and hydrological-models. *WATCH technical report 22* (2010). URL
235 <http://www.eu-watch.org/publications>.
- 236 22. Weedon, G. P. *et al.* The wfdei meteorological forcing data set: Watch forcing data methodol-
237 ogy applied to era-interim reanalysis data. *Water Resources Research* **50**, 7505–7514 (2014).
238 URL <http://dx.doi.org/10.1002/2014WR015638>.

- 239 23. Goodrich, L. The influence of snow cover on the ground thermal regime. *Canadian geotech-*
240 *nical journal* **19**, 421–432 (1982).
- 241 24. Nelson, F. E. Permafrost distribution in central canada: Applications of a climate-based pre-
242 dictive model. *Annals of the Association of American Geographers* **76**, 550–569 (1986). URL
243 <http://www.jstor.org/stable/2562710>.
- 244 25. Taylor, K. E., Stouffer, R. J. & Meehl, G. A. A summary of
245 the cmip5 experiment design. *PCMDI Tech. Rep.* (2009). URL
246 http://cmip-pcmdi.llnl.gov/cmip5/docs/Taylor_CMIP5_design.pdf.
- 247 26. Stocker, T. *et al.* *Climate Change 2013: The Physical Science Basis. Contri-*
248 *bution of Working Group I to the Fifth Assessment Report of the Intergovernmen-*
249 *tal Panel on Climate Change.* IPCC (Cambridge University Press, 2013). URL
250 <http://www.climatechange2013.org/>.
- 251 27. Xie, Y., Liu, Y. & Huang, J. Overestimated arctic warming and underestimated eurasia mid-
252 latitude warming in cmip5 simulations. *International Journal of Climatology* (2016). URL
253 <http://dx.doi.org/10.1002/joc.4644>.
- 254 28. Center for International Earth Science Information Network, C. I. E. S. I. N., Columbia Uni-
255 versity, C. U., International Food Policy Research Institute, I. F. P. R. I., The World Bank,
256 T. W. B. & Centro Internacional de Agricultura Tropical, C. I. A. T. Global rural-
257 urban mapping project, version 1 (grumpv1): Population density grid. *Palisades,*

- 258 NY: NASA Socioeconomic Data and Applications Center (SEDAC). (2011). URL
259 <http://dx.doi.org/10.7927/H4R20Z93>.
- 260 29. Balk, D. *et al.* Determining global population distribution: Methods, ap-
261 plications and data. *Advances in Parasitology* **62**, 119–156 (2006). URL
262 [http://dx.doi.org/10.1016/S0065-308X\(05\)62004-0](http://dx.doi.org/10.1016/S0065-308X(05)62004-0).
- 263 30. Shindell, D. & Faluvegi, G. Climate response to regional radiative forcing
264 during the twentieth century. *Nature Geoscience* **2**, 294–300 (2009). URL
265 http://www.nature.com/ngeo/journal/v2/n4/supinfo/ngeo473_S1.html.
- 266 31. Miller, G. H. *et al.* Arctic amplification: can the past constrain the fu-
267 ture? *Quaternary Science Reviews* **29**, 1779 – 1790 (2010). URL
268 <http://www.sciencedirect.com/science/article/pii/S0277379110000405>.
269 Special Theme: Arctic Palaeoclimate Synthesis (PP. 1674-1790).

270 **Supplementary Information** is linked to the online version of the paper.

271 **Acknowledgements** The authors acknowledge funding and support from the Permafrost in the Arctic and
272 Global Effects in the 21st century (PAGE21) Framework 7 project GA282700. S.E.C, G.H and S.W. were
273 funded under the Joint Partnership Initiative (JPI) project CONstraining Uncertainties in the Permafrost-
274 climate feedback (COUP) (S.E.C: National Environment Research Council grant NE/M01990X/1; G.H:
275 Swedish Research Council grant no. E0689701; S.W: Research Council of Norway project no. 244903/E10).
276 E.J.B. was supported by the Joint UK DECC/Defra Met Office Hadley Centre Climate Programme (GA01101).

277 P.M.C. and P.F. acknowledge funding from CRESCENDO (EU project 641816). S.E.C. is grateful to the
278 University of Exeter for access to facilities. Thanks to David Pearson for helpful discussions.

279 **Competing Interests** The authors declare that they have no competing financial interests.

280 **Correspondence** Correspondence and requests for materials should be addressed to S.E.C. (email: s.e.chad-
281 burn@exeter.ac.uk).

282 **Author contributions** S.E.C. developed the techniques, made the calculations for future projections of
283 permafrost, and produced the plots and manuscript. S.W. and G.H. provided and analysed data for eval-
284 uation, along with advice and comments. E.J.B. extracted CMIP5 model data. P.M.C. came up with the
285 original idea to address this question. P.M.C., E.J.B. and P.F. provided advice, ideas and discussion through-
286 out the process. All authors contributed towards writing the manuscript.

287 **Methods**

288 **Deriving the relationship between permafrost and MAAT for observations.** The relationship
289 shown in Figure 1a is produced by combining the International Permafrost Association (IPA) map
290 ²⁰ with WATCH reanalysis air temperature data at 0.5° spatial resolution ^{21,22}. The IPA map defines
291 the boundaries of the permafrost zones: Continuous, >90% coverage; discontinuous, 50-90% cov-
292 erage; sporadic, 10-50% coverage; isolated patches, 0-10% coverage. We extracted the grid cells
293 from WATCH that corresponded to the spatial boundaries of these permafrost zones on the IPA
294 map, and also any grid cell within 100km of the boundary to account for uncertainties in the
295 boundary placement or in fractional coverage at the boundaries. We used 31 years of mean annual

296 air temperatures (1960-1990), corresponding to the approximate time period from which the in-
297 formation in the IPA map was compiled. We took a 5-year rolling mean of the air temperatures to
298 remove some of the interannual variability, since permafrost responds on a multi-annual timescale.
299 The air temperature data were fitted against the permafrost fractions at the corresponding zonal
300 boundaries (0%, 10%, 50% and 90%). The curve was fitted using least squares regression, and
301 taking the same functional form as in ¹⁹, with two free parameters. The curve follows cumulative
302 normal distribution functions (i.e. a predefined shape). However, in ¹⁹ only the 10% and 90%
303 points are fixed based on literature values. Note that our curves are based on a much larger num-
304 ber of permafrost fraction vs. MAAT points which are obtained from the IPA permafrost map.
305 Furthermore, these points cover a range of possible values from 0 to 90%, so that our estimates
306 are well constrained. See the Supplementary material for a detailed validation of this relationship
307 against observations and high-resolution modelling.

308 Due to their coarse resolution the 0.5° air temperatures do not resolve the southern mountain
309 ranges in Europe and North America and therefore show permafrost at a MAAT up to +14°C, at
310 which it certainly cannot exist, so we removed these mountain ranges from the IPA map before
311 fitting the curves.

312 The upper and lower curves in Figure 1a were derived by binning the grid cells according to
313 air temperature (1°C intervals) and taking the permafrost fractions for each grid cell in each bin.
314 In each air temperature bin, we took the upper 50% of permafrost fractions to fit the upper curve,
315 and the lower 50% to fit the lower curve. While this does not place the curves at the absolute
316 extremes of the data, it well captures the large-scale variability, as shown in Figure 1 and further

317 in Supplementary information.

318 **Permafrost area from the IPA map** The total permafrost area from the IPA map²⁰ was estimated
319 by assuming the fractional coverage in each permafrost zone falls at the centre of the zonal range.
320 The upper and lower bounds were estimated by assuming the maximum/minimum fraction in all
321 zones.

322 **Analysis of CMIP5 models.** Model-specific relationships between MAAT and permafrost were
323 estimated for the CMIP5 models²⁵. These were derived by taking a set of points from each model
324 grid, at 2° latitude/longitude intervals north of 50° latitude, and splitting these according to 1°C
325 intervals of MAAT. In each air temperature interval we calculated the fraction of points at which
326 permafrost was simulated. For consistency with the observations, we took these values from the
327 historical simulations from 1960-1990. The limiting curves were estimated by taking the 50% of
328 points with the warmest and coldest soil temperatures for a given MAAT interval. This is very
329 similar to the derivation of upper and lower bounds for the observed relationship, except that in
330 the observations only the permafrost fraction is known, whereas in the models only a single soil
331 temperature is simulated for each grid cell.

332 The MAAT-permafrost curves for the CMIP5 models (equivalent to Figure 1a) are shown
333 in Figure S3. The variety of different MAAT-permafrost relationships show the discrepancies
334 in model representations of permafrost due to the inclusion/neglect of such processes as snow
335 insulation, thermal inertia and latent heat. This results in relative curve shifts of up to 10°C, and
336 curve gradients that vary from almost vertical to very shallow curves e.g. in NorESM1.

337 For future assessments we used the models that run stabilisations to 2300 for RCP4.5 and
338 RCP2.6. We do not include RCP8.5 in this analysis: Firstly there are very few CMIP5 models that
339 ran to 2300 with RCP8.5, and almost exclusively the warming is so high in these runs that there is
340 no permafrost remaining, which prevents further analyses of the MAAT to permafrost relationship.

341 To use our approach, it is important that the same relationships apply under equilibrium
342 conditions, and we verify this in the models on Figure S4, where we plot the MAAT-permafrost
343 curves at stabilisation at 2300, along with those derived from the historical simulations from 1960-
344 1990. In fact, there are some small differences in some of the models, but these are also the models
345 with the largest uncertainty bounds on the curve and thus the relationships at equilibrium fall within
346 the plausible range.

347 **Projection of future air temperatures.** To estimate the future air temperatures we increased the
348 historical air temperatures by the global mean warming, multiplied by an Arctic amplification fac-
349 tor. The amplification factor was derived as function of latitude, via a regression of air temperatures
350 over land, in 5° latitude bands, against the global mean air temperature, using WATCH reanalysis
351 air temperature data from 1936 to 2012 ^{21,22}.

352 The base air temperatures from which the air temperatures for different scenarios are derived,
353 using this pattern scaling approach, are taken from WATCH 1986-2005 20 year mean. At this time
354 global warming is assumed to be 0.61°C ²⁶.

355 The Arctic amplification uncertainty was estimated using the CMIP5 models, by comparing
356 the amplification factors in their historical simulation with their future simulation. By combining

357 all the models together we derived a full spatial covariance matrix of uncertainties.

358 Uncertainties for the final constraint were combined from taking upper and lower curves from
359 the permafrost-MAAT relationship, and from the Arctic amplification covariance matrix. For the
360 permafrost-MAAT curves we cannot calculate the spatial covariance, so we assume the maximum
361 (minimum) permafrost area is when every grid cell falls on the upper (lower) curve. To combine
362 with the amplification uncertainties, we assume that these limits correspond to 2σ . This approach
363 gives an upper limit on the uncertainty: While the permafrost-MAAT relationship varies locally
364 and for a given location it can shift under climatic changes (e.g. drier summers), the chances that it
365 will fall on either the upper or lower curve across the whole Arctic are extremely small. We include
366 such variability in the uncertainty bounds rather than explicitly resolving it, because the future
367 changes and even the present-day variability (since, for example, sub-surface characteristics are
368 not recorded in detail on global scales) are not yet well understood. The sensitivity of permafrost to
369 warming, and corresponding uncertainty bounds, were calculated from the 2° stabilisation relative
370 to pre-industrial levels.

371 The future Arctic amplification is subject to a lot of uncertainty. Figure S5 shows the ampli-
372 fication factors as a function of latitude in the models and observations, over the same historical
373 period. The historical amplification factor derived from the air temperature record is qualitatively
374 different than in most models ²⁷ (Fig. S5), suggesting that models may be failing to represent or
375 misrepresenting some processes. On the other hand, observations are sparse in the very high lati-
376 tudes, so it may arguably be more reliable to use models for this region. In practice, since models
377 and observations overlap in the very high latitudes, it does not make a large difference whether

378 we choose to use the observed or simulated values. We argue that while observations are sparse,
379 they are less likely to have a consistent bias, which the models clearly have since they consistently
380 disagree with the observations in the mid-northern latitudes, where observed data is quite reliable.
381 Therefore we choose to estimate the future Arctic amplification from historical observations, but
382 to use the models to give statistical uncertainty bounds (using spatial covariance of future amplifi-
383 cation).

384 It has been argued that Arctic amplification in future may be larger than over the last century,
385 since it has been suppressed over the last century by aerosol effects³⁰. Conversely, under very high
386 warming scenarios, sea ice and snow could largely disappear from the Arctic, leading to a reduction
387 in the albedo feedbacks and thus a reduced amplification effect. The future of permafrost under
388 the high warming scenarios is therefore somewhat uncertain (see Fig. 3). Further studies of Arctic
389 amplification in paleoclimate records may enable this constraint to be tightened³¹.

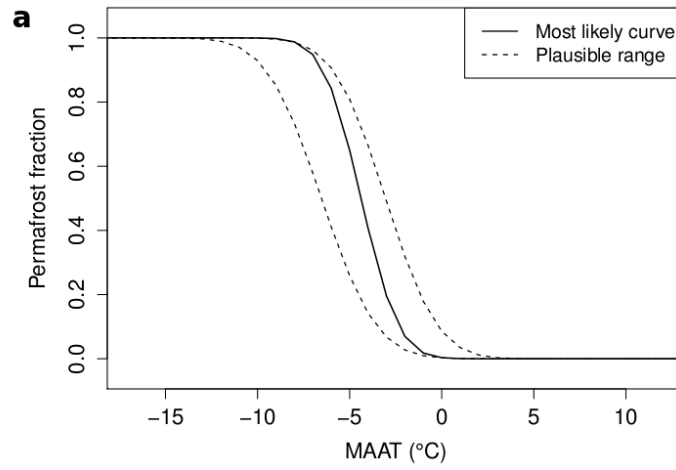
390 **Figure 1** Defining the spatial distribution of observed permafrost as a function of ob-
391 served air temperature. (a) Relationship between MAAT and permafrost fraction or prob-
392 ability. The central curve gives the most likely value, with upper and lower curves giving
393 the plausible range. See Fig. S1 for parameter values. (b-e) Permafrost distribution esti-
394 mated from reanalysis air temperatures and relationships in (a) (central curve (c), lower
395 curve (d), upper curve (e)) validated against the IPA map (b) ²⁰.

396 **Figure 2** Comparison of our estimate of global permafrost area with that simulated by
397 the CMIP5 models (stabilisation runs at 2300). (a): Using local air temperature from the
398 models and the model-specific MAAT-permafrost relationships. (b): Using global temper-
399 ature from the models, Arctic amplification from each model's historical simulation and the
400 MAAT-permafrost relationships. Error bars show 2σ confidence.

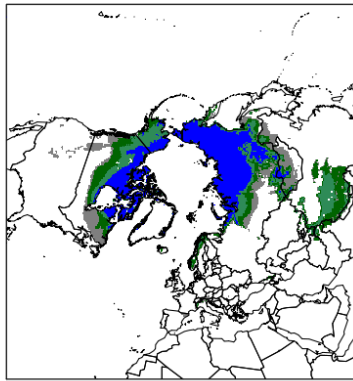
401 **Figure 3** Relationship between global warming stabilisation scenario and remaining
402 permafrost area using our approach. Boxes show 1σ and whiskers show 2σ uncertainty
403 bounds. Zero warming corresponds to pre-industrial climate (1850-1900 average). The
404 red box corresponds to the time-frame of the IPA permafrost map (Fig. 1b). The 'model'
405 points represent individual CMIP5 climate model stabilisation simulations (permafrost
406 area at 2300).

407 **Figure 4** Changes in spatial patterns of permafrost under future stabilisation scenarios.
408 The shaded areas show estimated historical permafrost distribution (1960-1990), and

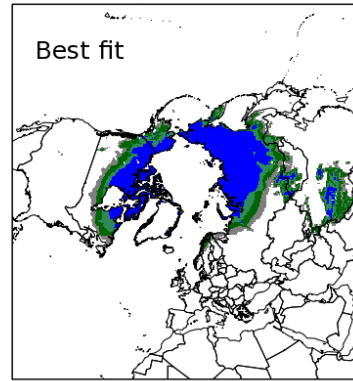
409 contours show the plausible range of zonal boundaries under 1.5°C stabilisation (a) and
410 under 2°C stabilisation (b).



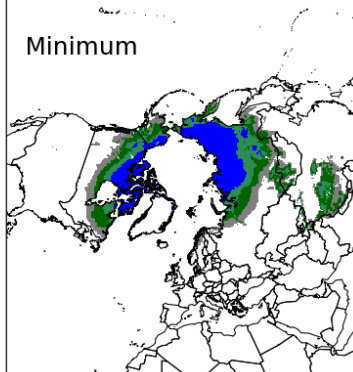
b Observations (Brown et al. 1998)



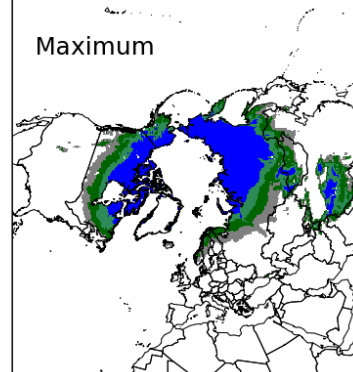
c From air temperatures, 1960–1990

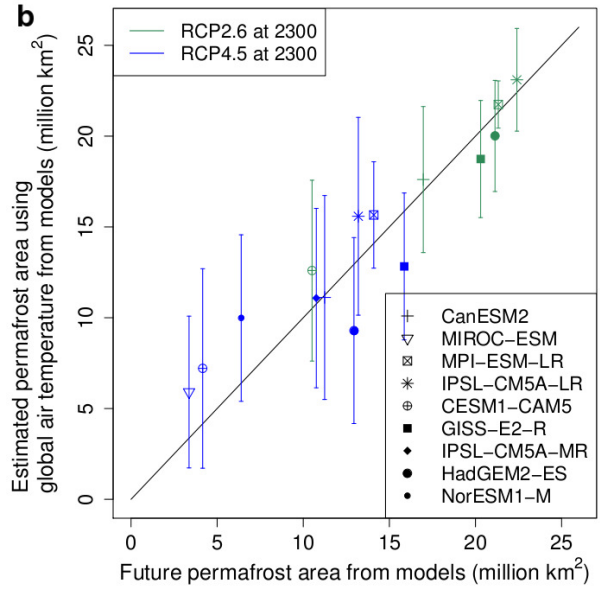
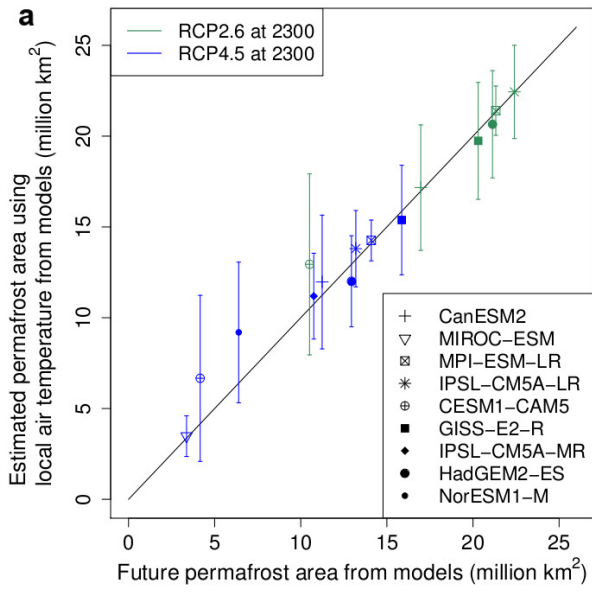


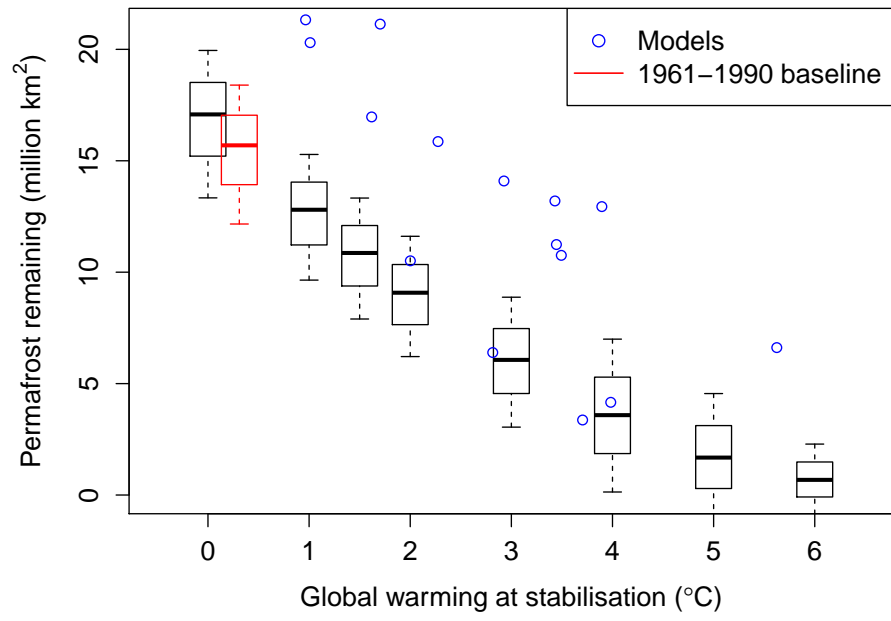
d From air temperatures, 1960–1990



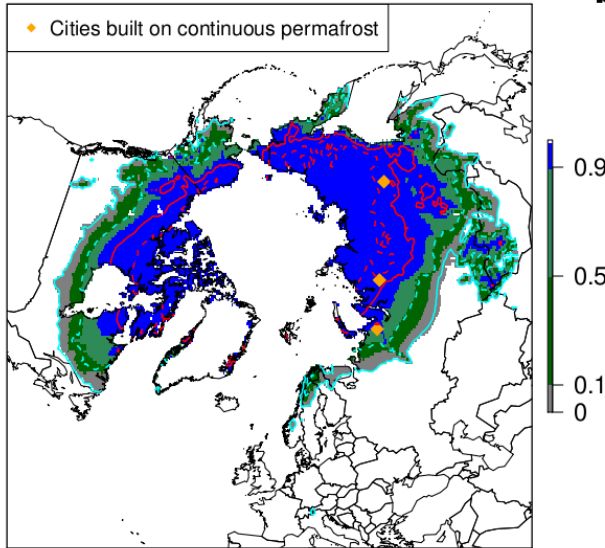
e From air temperatures, 1960–1990







a Changes in permafrost, 1.5°C warming



b Changes in permafrost, 2°C warming

